J. Phys. D: Appl. Phys. **30** (1997) 2462–2469. Printed in the UK PII: S0022-3727(97)81740-8

Statistical analysis of a mixed-layer x-ray diffraction peak

L Rebollo-Neira†, A G Constantinides†, A Plastino‡, A Alvarez§, R D Bonetto§ and A M Iñiguez-Rodriguez‖

† Department of Electrical and Electronic Engineering, Imperial College, Exhibition Road, London SW7 2BT, UK
‡ Departamento de Física, Universidad Nacional de La Plata, CC 67, 1900 La Plata, Argentina
§ Centro de Investigación y Desarrollo en Procesos Catalíticos, Calle 47 257, CC 59, 1900 La Plata, Argentina
‖ Centro de Investigaciones Geológicas, Calle 1 644, 1900 La Plata, Argentina

Received 10 February 1997, in final form 16 May 1997

Abstract. A mathematical model to describe the line shape of an x-ray diffraction peak from stacks of different layers such as, for instance, an interstratified clay mineral has been evolved. The aim was to be able to analyse the proportions of different specific stacking sequences in two-component interstratified samples. A maximum-entropy algorithm was applied to observed powder-diffraction intensities in order to obtain the probability of each stacking sequence. Application to natural smectite–illite clays gave reasonable results.

1. Introduction

The kinematical description (the single-scattering approximation) of the diffraction of x-rays by a crystal allows for a theory of diffraction which is known to be valid within the limit of *small crystals* [1]. In this paper we apply such a description in order to model the diffraction peak produced by the scattering of x-rays impinging on an interstratified stack. These materials differ from *small crystals* in that, since the diffracting stack is composed of layers of different types, its charge density is non-periodic in one direction and therefore, *strictu sensu*, the stack is not a crystal. The assumption of *small crystals* that guarantees the validity of the kinematical approximation is kept here *under the requirement of considering the number of layers that compose the corresponding stack small*.

The motivation for this work is that of facilitating the determination of stacking-sequence distributions in mixed-layer (interstratified) clay minerals. The seminal early work on interstratified clay (IC) minerals was that by Weaver, published in 1956 [2]. The pertinent modern literature is rather extensive, [3] providing one with a good summary.

Any investigation of mixed-layer clays (be they petrological or mineralogical in nature) critically depends on the ability to interpret their x-ray diffraction peaks [4]. We shall present here a framework that allows the observed x-ray diffraction peak to be modelled as arising from the contributions due to each interstratified stack (for every conceivable stacking sequence), weighted according to the distribution of sequences. Since the dimension of the pertinent configuration space is very large, compared with the information that can be directly obtained from the available diffraction measurements, recourse to the maximum-entropy principle is to be recommended [5–7].

The paper is organized in the following fashion. In section 2 the maximum-entropy approach is described, whereas section 3 deals with the particular case of mixed-layer systems of two components. Illustrations of the concomitant formalism are discussed in section 4, in which relevant realistic situations are considered. Finally, some conclusions are drawn in section 5.

2. The maximum-entropy approach

Here, we consider the analysis of the diffraction intensity coming from an interlayering of l different types of layer. The intensity distribution in the x-ray diffraction peaks is sensitive to the proportions of each different stacking sequence, so we will apply a maximum-entropy method to determine sequence distributions from intensities. In order to obtain this information we need to ascertain the response of a given sequence when x-rays of wavelength λ (of the order of the interplanar distance) impinge upon an appropriate sample.

Consider an interstratified stack that is formed by stacking up N layers. The position of each layer, along the stacking direction, will be labelled with an integer j that runs form one to N. Because we are dealing with l different types of layer we have l^N possible sequences. Let ν stand for the set of indices needed to specify a given sequence. Using the single-scattering approximation [1], the diffraction intensity $F_\nu(\theta)$ produced by a stack in the

0022-3727/97/172462+08$19.50

configuration ν turns out to be

$$F_\nu(\theta) \propto \sum_{i=1}^{N} H^2(i) + 2\sum_{i<j}^{N} H(i)H(j)\cos\left(\phi(j)-\phi(i) + \frac{4\pi}{\lambda}\sum_{s=1}^{j-1}(R(s+1)-R(s))\right) \tag{2.1}$$

where $R(j)$ is the distance from the site j to the detector, while $H(j)$ and $\phi(j)$ are, respectively, the modulus and phase of the pertinent structure factor, which will depend upon the type of layer located at the site j.

Consider now that the number N of layers per stack is not fixed but can run from one to N_m. Then, the number of all possible sequences in the sample, N_c, say, is

$$N_c = \sum_{N=1}^{N_m} l^N = \frac{l^{N_m+1}-l}{l-1}.$$

The probability of the sequence ν will be denoted by ρ_ν.

We assume that we have at our disposal the results of M diffraction measurements performed upon an l-component sample. Considering that the measurement I_k is performed at the angle θ_k, we write

$$I_k = I(\theta_k) = A\sum_{N=1}^{N_m}\sum_{\nu=1}^{l^N}\rho_\nu F_\nu(\theta_k) + B + e_k \qquad k = 1,\ldots,M \tag{2.2}$$

where the proportionality factor A allows for introduction of the normalization condition

$$\sum_{N=1}^{N_m}\sum_{\nu=1}^{l^N}\rho_\nu = 1 \tag{2.3}$$

and the constant B is used to represent the effects of a constant background. The terms e_k are 'noise' ones. Let e_k with $k = 1,\ldots,M$ be independent random variables, normally distributed with zero mean and variance σ_k^2 and define the quadratic form

$$\Psi(\rho_1,\ldots,\rho_{N_c},B) = \sum_{k=1}^{M}\frac{(I_k - A\sum_{N=1}^{N_m}\sum_{\nu=1}^{l^N}\rho_\nu F_\nu(\theta_k) - B)^2}{\sigma_k^2}. \tag{2.4}$$

The estimator of maximum likelihood is obtained by minimizing (2.4) and renders the classical generalized least-square solution. However, since we are dealing with a problem in which the number of unknowns is larger than the number of data, we are in the presence of an undetermined least-square problem. In general, the unrestricted minimization of (2.4) leads to solutions for which $\Psi(\rho_1,\ldots,\rho_{N_c},B)$ vanishes on a hyperplane (of dimension (N_c+1-M)) whose equation is given by (2.2) with $e_k = 0$ with $k = 1,\ldots,M$. In order to incorporate into the desired solution the restriction of positivity, but in a manner compatible with the nature of the errors affecting the data, we shall build a maximum-entropy solution that fixes a numerical value of $\Psi(\rho_1,\ldots,\rho_{N_c},B)$ that is only decided upon by *actually taking into account the errors in the data*. This is achieved by means of the iterative algorithm proposed in [6, 7], whose operational steps we describe below.

We start by determining the appropriate generalized least-square equations, that are obtained by demanding that

$$\frac{\partial\Psi}{\partial\rho_\nu} = 0 \qquad \nu = 1,\ldots,N_c \tag{2.5}$$

$$\frac{\partial\Psi}{\partial B} = 0. \tag{2.6}$$

Conditions (2.5) and (2.6) are tantamount to solving the equations

$$T_\mu = A\sum_{N=1}^{N_m}\sum_{\nu=1}^{l^N}\rho_\nu a_{\nu,\mu} \qquad \mu = 1,\ldots,N_c \tag{2.7}$$

where

$$T_\mu = \sum_{k=1}^{M}\frac{I_k F_\mu(\theta_k)}{\sigma_k^4} - \left(\sum_{k=1}^{M}\frac{I_k}{\sigma_k^4}\right)\left(\sum_{k=1}^{M}\frac{F_\mu(\theta_k)}{\sigma_k^4}\right)\times\left(\sum_{k=1}^{M}\frac{1}{\sigma_k^4}\right)^{-1} \tag{2.8}$$

$$a_{\nu,\mu} = \sum_{k=1}^{M}\frac{F_\mu(\theta_k)F_\nu(\theta_k)}{\sigma_k^4} - \left(\sum_{k=1}^{M}\frac{F_\mu(\theta_k)}{\sigma_k^4}\right)\times\left(\sum_{k=1}^{M}\frac{F_\nu(\theta_k)}{\sigma_k^4}\right)\left(\sum_{k=1}^{M}\frac{1}{\sigma_k^4}\right)^{-1}. \tag{2.9}$$

The system of equations (2.7) is, of course, redundant. In order to eliminate this redundancy we use these equations, in successive fashion (one by one), as constraints to be satisfied by a maximum-entropy solution. Accordingly, if several (indeed an infinite number) ρ_ν are candidates that fulfil the given constraints, the one to be selected is that which maximizes the statistical entropy S [8–10]

$$S = -\sum_{N=1}^{N_m}\sum_{\nu=1}^{l^N}\rho_\nu\ln\rho_\nu. \tag{2.10}$$

We regard each T_μ in (2.7) as proportional to the mean value of a random variable that adopts the values $a_{\nu,\mu}$ with $\nu = 1,\ldots,N_c$ with probability ρ_ν and we solve the set of equations (2.7) in an iterative manner. In order to estimate the unknown constant A we choose just one of the equations (2.7), the αth say, so that we have

$$A = T_\alpha\left(\sum_{N=1}^{N_m}\sum_{\nu=1}^{l^N}\rho_\nu a_{\nu,\alpha}\right)^{-1} \tag{2.11}$$

and the system to be solved can be re-cast in the form

$$\sum_{N=1}^{N_m}\sum_{\nu=1}^{l^N}\rho_\nu Q_{\nu,\mu} = 0 \qquad \mu\neq\alpha;\ \mu = 1,\ldots,N_c \tag{2.12}$$

where

$$Q_{\nu,\mu} = T_\alpha a_{\nu,\mu} - T_\mu a_{\nu,\alpha}. \tag{2.13}$$

We start the iterative process now by employing the maximum-entropy principle in each step. The zeroth-order approximation is devised by requiring that the zeroth-order distribution $\rho_\nu^{(0)}$ maximizes the entropy (2.10) with the

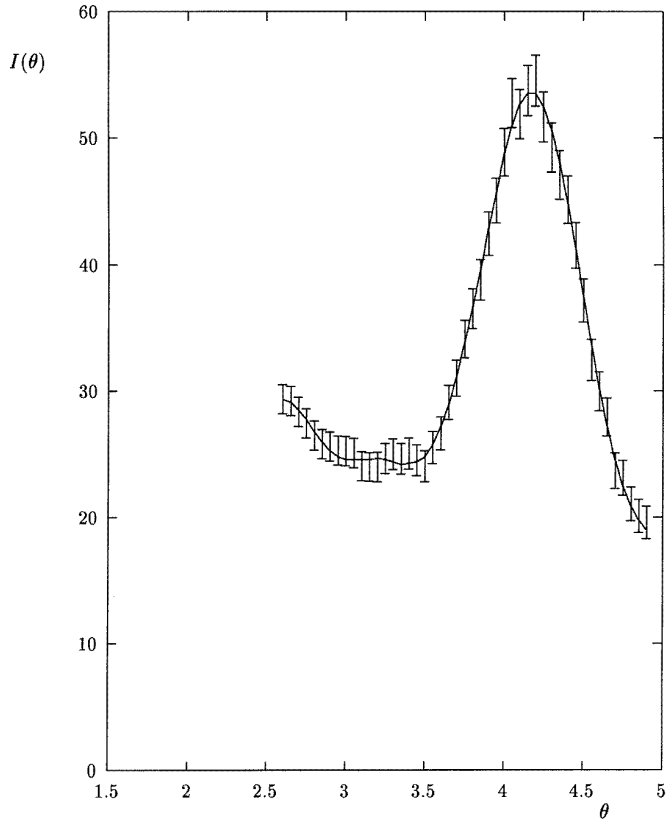

Figure 1. X-ray diffraction intensities (arbitrary units) versus the diffraction angle. The full curve corresponds to the $\rho_{\nu 1}^{(6)}$ theoretical predictions.

normalization constraint only. This entails $\rho_\nu^{(0)} = 1/N_c$ and the zeroth-order estimate for A is then

$$A^0 = T_\alpha \left(\sum_{N=1}^{N_m} \sum_{\nu=1}^{l^N} \frac{a_{\nu,\alpha}}{N_c} \right)^{-1} \tag{2.14}$$

so that we predict a zeroth-order value for the T_μ as given by

$$T_\mu^0 = T_\alpha \sum_{N=1}^{N_m} \sum_{\nu=1}^{l^N} a_{\nu,\mu} \left(\sum_{N=1}^{N_m} \sum_{\nu=1}^{l^N} a_{\nu,\alpha} \right)^{-1} \qquad \mu = 1, \ldots, N_c. \tag{2.15}$$

The quality of these conjectures is measured in terms of 'predictive errors' ϵ_μ that are defined in the fashion

$$\epsilon_\mu = \frac{|T_\mu - T_\mu^0|}{|T_\mu|} \qquad \mu = 1, \ldots, N_c \tag{2.16}$$

where the T_μ with $\mu = 1, \ldots, N_c$ are given by (2.8). Let μ_1 be the index such that $\epsilon_{\mu_1} \geq \epsilon_\mu$ with $\mu = 1, \ldots, N_c$. The first-order distribution $\rho_\nu^{(1)}$ is then obtained by maximizing (2.10) subject to the constraint

$$\sum_{N=1}^{N_m} \sum_{\nu=1}^{l^N} \rho_\nu^{(1)} Q_{\nu,\mu_1} = 0 \tag{2.17}$$

which is equivalent to enforcing the fulfilment of the μ_1th equation in the system (2.7). This, plus the normalization requirement (2.3), leads to

$$\rho_\nu^{(1)} = \frac{\exp(-\lambda_1 Q_{\nu,\mu_1})}{\sum_{N=1}^{N_m} \sum_{N=1}^{l^N} \exp(-\lambda_1 Q_{\nu,\mu_1})} \tag{2.18}$$

where the Lagrange multiplier λ_1 is obtained by solving (2.17). With $\rho_\nu^{(1)}$ we obtain a first-order estimation for the parameters A and B (let us call them $A^{(1)}$ and $B^{(1)}$), so that we can build the 'predictions' $T_\mu^{(1)}$ with $\mu = 1, \ldots, N_c$. From these predictions we calculate the concomitant (new) set $\{\epsilon_\mu\}$. After we have selected the largest one, ϵ_{μ_2}, say, we obtain $\rho_\nu^{(2)}$ by maximizing S subject to two constraints, namely, the fulfilment of the equations in the set (2.12) corresponding both to $\mu = \mu_1$ and to $\mu = \mu_2$.

The following steps continue in the same fashion by selecting from the set (2.7) the 'worst' result and using it as the constraint for the next iterative step. Following such a procedure, the Jth-order approximation is given by

$$\rho_\nu^{(J)} = \frac{\exp(-\sum_{i=1}^{J} \lambda_i Q_{\nu,\mu_i})}{\sum_{N=1}^{N_m} \sum_{\nu=1}^{l^N} \exp(-\sum_{i=1}^{J} \lambda_i Q_{\nu,\mu_i})} \tag{2.19}$$

where the Lagrange multipliers λ_i with $i = 1, \ldots, J$ are obtained by solving the J equations

$$\sum_{N=1}^{N_m} \sum_{\nu=1}^{l^N} \rho_\nu^{(J)} Q_{\nu,\mu_i} = 0 \qquad i = 1, \ldots, J. \tag{2.20}$$

At each step, say, up to the Jth-order approximation, we can make definite predictions concerning the result of

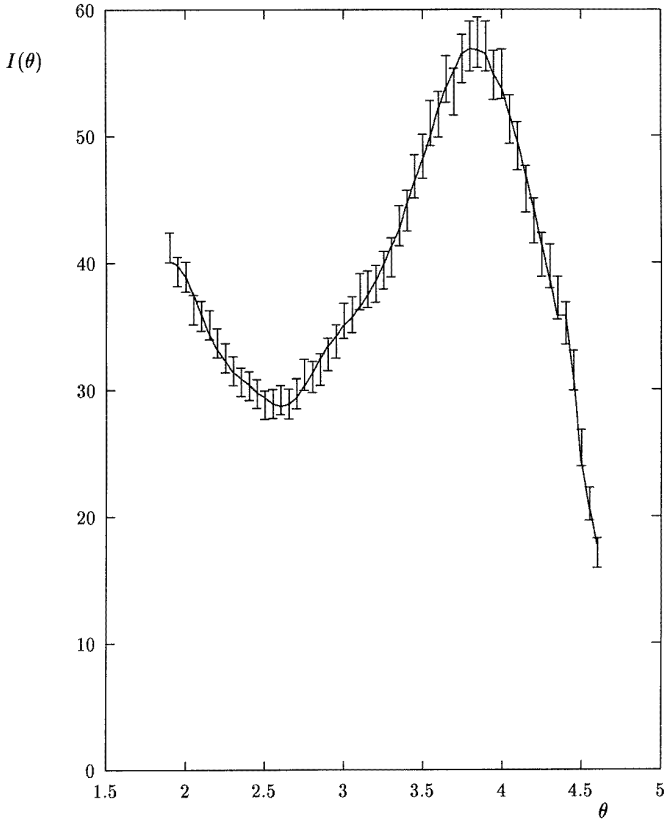

Figure 2. The same details as in figure 1, but that the full curve corresponds to the $\rho_{\nu 2}^{(10)}$ theoretical predictions.

diffraction measurements $I_k^{(J)}$. Indeed,

$$I_k^{(J)} = A^{(J)} \sum_{N=1}^{N_m} \sum_{\nu=1}^{l^N} \rho_\nu^{(J)} F_\nu(\theta_k) + B^{(J)} \qquad k = 1, \ldots, M \tag{2.21}$$

where

$$A^{(J)} = T_\alpha \left(\sum_{N=1}^{N_m} \sum_{\nu=1}^{l^N} \rho_\nu^{(J)} a_{\nu,\alpha} \right)^{-1} \tag{2.22}$$

$$B^{(J)} = \left(\sum_{k=1}^{M} \frac{I_k}{\sigma_k^4} - A^{(J)} \sum_{N=1}^{N_m} \sum_{\nu=1}^{l^N} \rho_\nu^{(J)} \sum_{k=1}^{M} \frac{F_\nu(\theta_k)}{\sigma_k^4} \right) \times \left(\sum_{k=1}^{M} \frac{1}{\sigma_k^4} \right)^{-1}. \tag{2.23}$$

The algorithm is to be stopped when these predictions are such that

$$|I_k^{(J)} - I_k| \leq \Delta I_k \qquad k = 1, \ldots, M \tag{2.24}$$

where ΔI_k are estimated as $\Delta I_k = 2\sigma_k$. Since the data are known only within the uncertainty ΔI_k, when that particular stage is reached for which (2.24) is verified, we will have used all the information at our disposal in order to check the predictive power of the maximum-entropy solution. The quadratic form (2.4) will then be $\Psi(\rho_1^{(J)}, \ldots, \rho_{N_c}^{(J)}, B) \neq 0$, which should account for the experimental errors.

Let us suppose that the acceptability test (2.24) is satisfied at the Lth iteration. At that point, $\rho_\nu^{(L)}$ can be employed to determine the relative quantities of the materials in the sample, namely

$$\langle N^i \rangle = \sum_{N=1}^{N_m} \sum_{\nu=1}^{l^N} \rho_\nu^{(L)} N_\nu^i \tag{2.25}$$

where N_ν^i with $i = 1, \ldots, l$ is the number of layers of type i in the configuration ν.

3. The two-component mixed-layering problem

Interlayered, mixed-layer or interstratified phyllosilicates are those in which two or more different types of layer are stacked together along the axis normal to (001). Phyllosilicate layers are strongly bonded internally, but rather weakly to each other. The basal surfaces of different kinds of layers are geometrically very similar, consisting of sheets of oxygen or hydroxyl ions disposed in a pseudo-hexagonal array [11]. The combination of weak interlayer bonding and structural commensuration parallel to the layers allows the observed interstratification.

Although interstratifications of more than two components have been reported [2, 12, 13], we will deal here only with two-component systems (layer 1 and layer 2). Layer 1 is characterized by (i) an interplanar spacing d_1 and (ii) a structure factor whose modulus and phase depend both on the diffraction angle θ and are denoted by $H_1(\theta)$ and $\phi_1(\theta)$, respectively. Accordingly, the corresponding figures for layer 2 are denoted by d_2, $H_2(\theta)$ and $\phi_2(\theta)$, respectively.

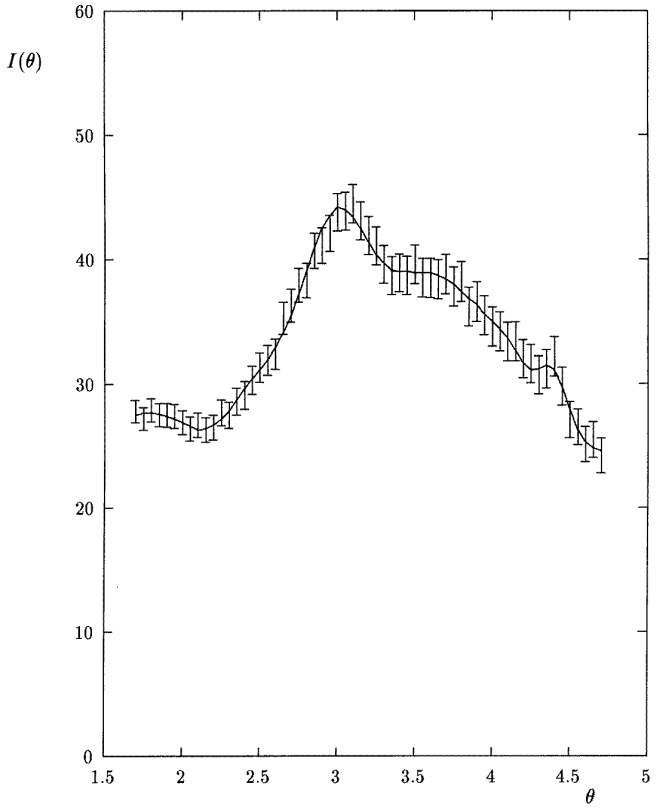

Figure 3. The same details as in figure 1, but that the full curve corresponds to the $\rho_{\nu 3}^{(11)}$ theoretical predictions.

The diffraction intensity resulting from a 001-oriented stack of N layers arranged in a vertical sequence perpendicular to the 001 plane is given by (2.1). The detailed aspect of (2.1) is determined by the occupational sequence. In this instance one has

$$H(j) = \begin{cases} H_1(\theta) & \text{if site } j \text{ corresponds to a layer of type 1} \\ H_2(\theta) & \text{if site } j \text{ corresponds to a layer of type 2} \end{cases} \tag{3.1}$$

$$\phi(j) = \begin{cases} \phi_1(\theta) & \text{if site } j \text{ corresponds to a 1-layer} \\ \phi_2(\theta) & \text{if site } j \text{ corresponds to a 2-layer} \end{cases} \tag{3.2}$$

$$R(j+1) - R(j) = \begin{cases} d_1 \sin(\theta) & \text{if both sites } (j \text{ and } j+1) \text{ correspond to a 1-layer} \\ d_2 \sin(\theta) & \text{if both sites correspond to a 2-layer} \\ \dfrac{(d_1+d_2)}{2} \sin(\theta) & \text{if both types of layers are involved.} \end{cases} \tag{3.3}$$

As stated in section 2, we have N layers for each stack and thus we are dealing with 2^N possible sequences per stack, N ranging from unity up to a maximum value N_m. Remember that ν stands for the set of indices needed to specify a given configuration, that $F_\nu(\theta)$ is the value of (2.1) for configuration ν and that the probability of finding the sequence ν in our sample is denoted by ρ_ν. We are now in a position to write down the expression for our all-important quantity: the measured diffraction intensity at the angle θ, that will be of the form

$$I(\theta) = A \sum_{N=1}^{N_m} \sum_{\nu=1}^{2^N} \rho_\nu F_\nu(\theta) + B. \tag{3.4}$$

We have introduced at this point all the elements needed in order to tackle an involved, realistic problem in the forthcoming section, in which specific examples of two-component systems are to be addressed.

4. The application to natural illite–montmorillonite samples

Montmorillonite is a smectite clay that easily exchanges cations with other substances [11, 14]. We shall analyse here results concerning sodic montmorillonite samples, in which Na cations *between the layers* compensate for lattice (charge) defects.

Illite clays may originate from montmorillonite and are not able to exchange cations. They rarely appear in pure, single-phase states. Some degree of interstratification is often present, hence it is of great geological and industrial interest to learn details about this interstratification. As

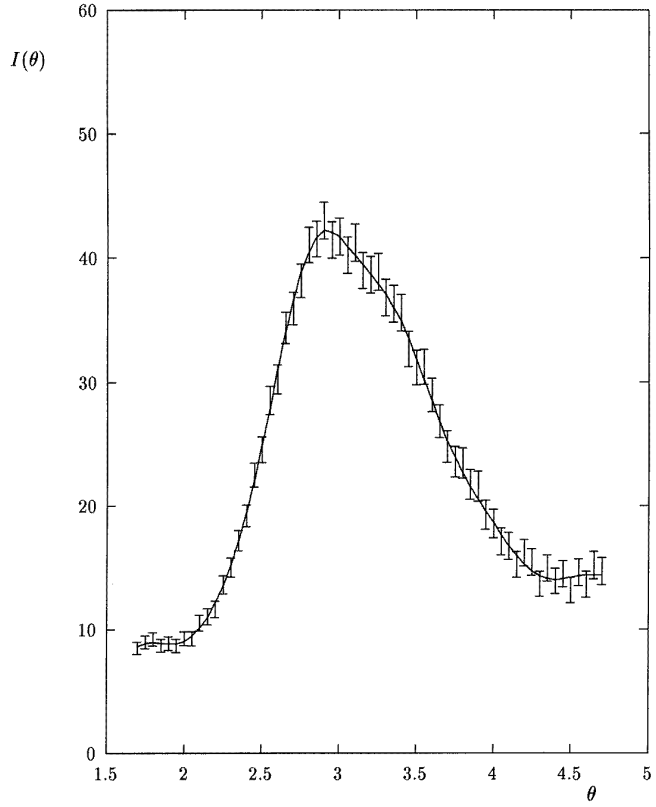

Figure 4. The same details as in figure 1, but that the full curve corresponds to the $\rho_{\nu 4}^{(11)}$ theoretical predictions.

an example we may mention that interstratification details are of importance in the determination of diagenetic zones. They are intimately related both to the origin and to the migration of hydrocarbons in a sedimentary basin.

From a petrological standpoint illite–smectites are the most interesting mixed-layer clays. They are quite ubiquitous, well known from a chemical standpoint and exhibit a mineralogical variation that responds to pressure–temperature variations during diagenesis [15–17].

In order to understand the transformation from smectite to illite that takes place during diagenesis and consequently to establish its role during the transformation of organic matter into liquid and gaseous hydrocarbons, it is of great interest to be in a position to determine the relative proportions of smectite and illite in ICs, as well as the concomitant distribution of stacking sequences.

We shall apply the considerations of the previous sections to this situation and assign label 1 to montmorillonite and label 2 to illite ($d_1 = 15.8$ Å and $d_2 = 10$ Å). We take the montmorillonite structure factors from [18], whereas those for illite were computed from the structure reported in [19].

Figures 1–4 display x-ray diffraction peaks obtained from illite–montmorillonite polycrystalline samples (these data have already been corrected for the Lorentz-polarization factor). The error bars in these figures are drawn assuming a 2σ error in the measurement of intensities, where $\sigma = (I)^{\frac{1}{2}}$ (I is the measured intensity). The samples were prepared so as to be preferentially oriented according to the $00l$ direction. This is achieved by sedimentation from a water suspension onto a glass surface.

As a first example, we believe it to be instructive to analyse an illite sample which is known to be in a single phase (that is, a sample with a negligible degree of interstratification). In previous works [20, 21], it was shown that the particle size distribution of sodic montmorillonite samples was such that most stacks had fewer than six layers. For this reason (and according to the results arising from this first example) we shall consider $N_m = 10$ (which entails dealing with 2046 configurations) and we shall assume that configurations with more than ten layers are of the single-phase kind only (so that in the concomitant states the maximum number of layers can be safely set to be equal to 50).

Figure 1 displays x-ray diffraction measurements from the sample under consideration. We are dealing with 47 data points. In order to attain concordance for all of them with ΔI_k (see equation (2.24)), as represented by the error bars, it was found necessary to construct a sixth-order approximation through which the theoretical values are calculated according to the relations

$$I_k^{(6)} = A^{(6)} \sum_{N=1}^{10} \sum_{\nu=1}^{2^N} \rho_\nu^{(6)} F_\nu(\theta_k) + A^{(6)} \sum_{K=11}^{50} \rho_K^{(6)} F_K(\theta_k) + B^{(6)} \tag{4.1}$$

where the index K stands for the illite single-phase configurations corresponding to $N_m > 10$, that have been

Table 1. The most populated 50 configurations corresponding to the samples here analysed. The stacking distributions $\rho_{\nu 1}^{(6)}$, $\rho_{\nu 2}^{(10)}$, $\rho_{\nu 3}^{(11)}$ and $\rho_{\nu 4}^{(11)}$ are those of figures 1, 2, 3 and 4,respectively.

ν_1	$\rho_{\nu_1}^{(6)}$	ν_2	$\rho_{\nu_2}^{(10)}$	ν_3	$\rho_{\nu_3}^{(11)}$	ν_4	$\rho_{\nu_4}^{(11)}$
2222	0.253 16	2	0.0 9368	2222222	0.033 06	1111	0.116 55
222222	0.248 91	1	0.081 78	2222212	0.033 01	11	0.077 24
22222	0.235 74	221	0.078 31	2122222	0.033 01	1	0.063 99
222	0.098 31	122	0.078 31	2221222	0.032 36	2	0.053 12
2221222	0.065 67	222	0.076 66	222222	0.031 02	111	0.038 59
2222222	0.043 90	222222	0.064 32	222221	0.029 00	211	0.027 10
22222222	0.041 99	2222	0.047 90	122222	0.029 00	112	0.027 10
2	0.008 92	22122	0.040 10	2222	0.024 89	212	0.022 71
22	0.001 02	12222	0.036 27	212222	0.022 85	11221	0.015 99
222222222	0.000 42	22221	0.036 27	222212	0.022 85	12211	0.015 99
1222	0.000 23	22222	0.028 93	22222222	0.018 83	112211	0.013 60
2221	0.000 23	222221	0.022 64	1222212	0.018 55	22111	0.012 57
1	0.000 12	122222	0.022 64	2122221	0.018 55	11122	0.012 57
1221222	0.000 08	22222222	0.020 74	222122	0.016 97	1112111	0.011 57
2221221	0.000 08	12221	0.020 35	221222	0.016 97	1212211	0.011 23
222122	0.000 05	22	0.017 51	22212	0.015 95	1122121	0.011 23
221222	0.000 05	2222222	0.016 14	21222	0.015 95	11222	0.010 06
22221	0.000 03	222122	0.015 78	22222	0.015 29	22211	0.010 06
12222	0.000 03	221222	0.015 78	1222221	0.011 67	22	0.009 46
122222	0.000 02	2212222	0.013 78	222222222	0.011 64	111111	0.009 19
222221	0.000 02	2222122	0.013 78	2111222	0.010 32	122111	0.008 93
1222222	0.000 01	122221	0.007 63	2221112	0.010 32	111221	0.008 93
2222221	0.000 01	1222122	0.007 19	22	0.008 69	122122	0.007 43
12221	0.000 00	2212221	0.007 19	2221	0.008 01	221221	0.007 43
1221	0.000 00	2222221	0.005 47	1222	0.008 01	1112212	0.007 30
221221	0.000 00	1222222	0.005 47	212	0.007 83	2122111	0.007 30
122122	0.000 00	12122	0.004 54	211222	0.007 46	122122	0.006 85
221	0.000 00	22121	0.004 54	222112	0.007 46	221221	0.006 85
122	0.000 00	212222	0.003 37	212221	0.006 72	12212	0.006 78
2212222	0.000 00	222212	0.003 37	122212	0.006 72	21221	0.006 78
2222122	0.000 00	1221	0.003 05	2212	0.005 98	221	0.006 48
12212	0.000 00	121	0.002 87	2122	0.005 98	122	0.006 48
21221	0.000 00	2212121	0.002 59	12221	0.005 63	12111	0.006 34
22122	0.000 00	1212122	0.002 59	2112	0.005 53	11121	0.006 34
122221	0.000 00	11	0.002 04	2112222	0.005 46	1122	0.006 24
122212	0.000 00	1212221	0.001 94	2222112	0.005 46	2211	0.006 24
212221	0.000 00	1222121	0.001 94	2212121	0.005 34	12	0.005 15
22212	0.000 00	2212122	0.001 86	1212122	0.005 34	21	0.005 15
21222	0.000 00	122122	0.001 85	21112	0.005 31	11211	0.005 06
1222221	0.000 00	221221	0.001 85	12212	0.005 26	21111	0.004 99
12222221	0.000 00	1221211	0.001 83	21221	0.005 26	11112	0.004 99
1222212	0.000 00	1121221	0.001 83	12	0.005 23	1121221	0.004 92
2122221	0.000 00	2221222	0.001 75	21	0.005 23	1221211	0.004 92
21	0.000 00	21222	0.001 70	222	0.005 19	11111	0.004 82
12	0.000 00	22212	0.001 70	121	0.005 17	1112	0.004 42
2122	0.000 00	1212222	0.001 53	12222	0.005 16	2111	0.004 42
2212	0.000 00	2222121	0.001 53	22221	0.005 16	12121	0.004 19
212222	0.000 00	12	0.001 45	12121	0.005 08	1221	0.004 08
222212	0.000 00	21	0.001 45	212112	0.005 08	211111	0.004 07
11	0.000 00	2122	0.001 42	211212	0.005 08	111112	0.004 07

added in this particular case. As illustrated by the full curve in figure 1, these agree with the data within the experimental error. Thus, $\rho_{\nu}^{(6)}$ can be confidently employed to determine the relative quantities of montmorillonite and illite in the sample, given, respectively, by

$$\langle N^1 \rangle = \sum_{N=1}^{10} \sum_{\nu=1}^{2^N} \rho_{\nu}^{(6)} N_{\nu}^1 \tag{4.2}$$

$$\langle N^2 \rangle = \sum_{N=1}^{10} \sum_{\nu=1}^{2^N} \rho_{\nu}^{(6)} N_{\nu}^2 + \sum_{K=11}^{50} \rho_{K}^{(6)} N_{K}^2 \tag{4.3}$$

and one finds 99% for illite and 1% for montmorillonite (as had been expected *a priori*). In the first and second columns of table 1, the 'most populated' configurations are shown. It can be seen that the single-phase states are the only relevant ones in this sample and that, among them, those corresponding to small numbers of layers predominate. According to this result, for the following analysis we find it reasonable to maintain the same number N_m of layers as that employed in this case.

A second sample was analysed for which convergence (53 data points) was attained by recourse to an tenth-

order approximation. The full curve in figure 2 depicts the pertinent results. In this case, the relative quantities of illite and montmorillonite in the sample were found to be 80 and 20%, respectively. In the third and fourth columns of table 1 the most populated sequences corresponding to this sample are displayed.

Figure 3 plots the 63 data points that we deal with in order to analyse a third sample. The continuous curve shows the concordance we obtain by recourse to an 11th-order approximation, which determined 30% montmorillonite and 70% illite to be in the sample. Note that, although these relative percentages are not very different from those of the second sample, the pertinent diffraction peaks have quite distinct line shapes (figures 2 and 3). This is due to the fact that (as shown in the fifth and sixth columns of table 1), whereas in the second sample illite-rich configurations are favoured, there is no such preference in the third sample. Since in this case the few configurations shown in table 1 do not provide one with a good description of the different stacking sequences in the sample, some further comments are in order: of the 80% total illite percentage present in sample 3, 22% of it exists in a separate phase (that is, not in mixed layers), being responsible for the small peak that appears at 4.4° (figure 3). The percentage of montmorillonite as a separate phase is negligible even though the main maximum in figure 3 appears at 3.1° (namely in the vicinity of the x-ray peak for a separate montmorillonite phase at 2.85°). This is due to the fact that the montmorillonite structure factor at this last angle is larger (by a factor of four) than the corresponding illite structure factor at its characteristic angle of 4.4°.

The strong influence of montmorillonite single-phase states on the diffraction peak's shape is illustrated by the fourth sample analysed in this work. Figure 4 displays the 61 data points to be dealt with here. The continuous curve of figure 4 shows the convergence to the measurements we obtained through an 11th-order approximation which determined 60% of montmorillonite and 40% of illite to be present in the sample. As displayed in the seventh and eighth columns of table 1, this sample does contain montmorillonite single-phase states and their strong contribution to the diffraction peak can be recognized in figure 4.

5. Conclusions

A model for the angular variation of the diffracted x-ray intensity from small stacks of mixed layers has been evolved. A formalism has been presented that allows one to obtain a detailed analysis of the sample by stack size and specific stacking configuration. The theoretical framework deals with all possible stacking sequences on an impartial basis. The probability to be assigned to each sequence is determined *a posteriori*, by analysing the x-ray diffraction peak produced by the sample. To this end, a maximum-entropy-based method was applied in order to obtain the probability distribution that, whilst being consistent with the available data, is maximally noncommittal with respect to the missing information.

The proposed approach has been shown to reproduce with high accuracy previously known results (the first example). Therefore, we feel confident that our analysis can be reliably applied to different situations, some of which have been discussed in this paper.

Acknowledgments

L Rebollo-Neira is a member of the Scientific Staff of CICPBA (Comisión de Investigaciones Científicas de la Provincia de Buenos Aires) and acknowledges support from the CONICET. She wishes to express her gratitude to Dr T J Seller for his help and assistance during her stay in England. A Plastino, G Alvarez and R D Bonetto acknowledge support from the National Research Council (CONICET) of Argentina.

References

[1] James R W 1954 *The Crystallite State, Volume II: The Optical Principles of the Diffraction of X-rays* (London: Bell)
[2] Weaver C E 1956 *Am. Mineral.* **41** 202
[3] 1986 *Clays and Clay Minerals* (The Clay Minerals Society) **34** No 2
[4] Reynolds R C 1980 *Crystal Structures of Clays Minerals and their X-Ray Identification* ed G W Brindley and G Brown (London: Mineralogical Society) pp 249–303
[5] Plastino A, Rebollo-Neira L and Alvarez A G 1989 *Phys. Rev.* A **40** 1644
[6] Rebollo-Neira L and Plastino A 1993 *Maximum Entropy and Bayesian Methods* ed A Mohammed-Djafari and G Demoment (Dordrecht: Kluwer) pp 67–72
[7] Rebollo-Neira L, Constantinides A, Plastino A, Zyserman F, Alvarez A, Bonetto R and Viturro H 1993 *Physica* A **198** 514
[8] Jaynes E T 1957 *Phys. Rev.* **106** 620
[9] Jaynes E T 1979 *The Maximum Entropy Formalism* ed R D Levine and M Tribus (Boston, MA: MIT) pp 15–118
[10] Shannon C E 1948 *Bell Syst. Tech. J.* **27** 379–423
Shannon C E 1948 *Bell Syst. Tech. J.* **27** 623–56
[11] Brindley G W and Brown G 1980 *Crystal Structures of Clays Minerals and their X-Ray Identification* (London: Mineralogical Society)
[12] Jonas E C and Brown T E 1959 *J. Sedim. Petrol.* **29** 77
[13] Foscolos A E and Kodama H 1974 *Clays Clay Minerals* **22** 319
[14] Pinavia T 1983 *Science* **220** 365
[15] Burst J F 1969 *Am. Assoc. Petrol. Geol. Bull.* **53** 73
[16] Velde B 1969 *Bull. Soc. Fr. Minéral. Crist.* **92** 360
[17] Perry E and Hower J 1970 *Clays Clay Minerals* **18** 165
[18] Cole W F and Lancucki C J 1966 *Acta Crystallogr.* **21** 836
[19] Weaver C E and Pollard L D 1973 *The Chemistry of Clay Minerals* (Amsterdam: Elsevier)
[20] Guérin D M A, Alvarez G, Rebollo-Neira L, Plastino A and Bonetto R 1985 *Acta Crystallogr.* A **42** 30
[21] Alvarez G, Bonetto R D, Guérin D, Plastino A and Rebollo-Neira L 1987 *Powder Diffraction* **2** 220
[22] Klug H P and Alexander L E 1974 *X-ray Diffraction Procedures, for Polycrystalline and Amorphous Materials* 2nd edn (New York: Wiley)